International Journal of Micro Air Vehicles

ORIGINAL RESEARCH ARTICLE

Open Access

https://doi.org/10.48130/mav-0026-0014

International Journal of Micro Air Vehicles **2026**, 18: e013

Control barrier function-based obstacle avoidance and formation cooperative control for multi-UAV system with unknown disturbance

Xiaoyue Wang[1,2], Jiaxin Cao[3], Kun Yan[3*], Dawei Liu[2] and Jingliang Sun[1]

[1] *School of Aerospace Science and Technology, Beijing Institute of Technology, Beijing 100081, China*
[2] *China Academy of Ordnance Science, Beijing 100089, China*
[3] *School of Electronic Information Engineering, Xi'an Technological University, Xi'an 710021, China*
* Correspondence: yankun@xatu.edu.cn (Yan K)

Abstract

Combining the consensus theory and control barrier function (CBF) techniques, a formation anti-disturbance and obstacle avoidance scheme is proposed for a fixed-wing multiple unmanned aerial vehicle system (MUAVS). Firstly, the disturbed longitudinal dynamics model of MUAVS is established. Meanwhile, the interval disturbance observer (IDO) approach is adopted to tackle unknown disturbance, which enables it to cover all possible estimated values at any moment. In comparison with other disturbance rejection approaches, the proposed IDO can exhibit a precise estimation scope prior to the convergence of the estimation error. Subsequently, the CBF and quadratic programming technologies are combined to achieve autonomous obstacle avoidance and performance optimization for MUAVS. The proposed CBF-based approach outperforms the traditional artificial potential field (APF) method by providing a more rigorous derivation and avoiding the local minima problem. Relying on consensus theory, a formation and collision-avoidance strategy is constructed for MUAVS, and the tracking stability is rigorously proved. The effectiveness and improvement are verified through comparative simulations.

Keywords: MUAVS, Interval disturbance observer, Control barrier function, Formation obstacle avoidance, Consensus theory

Citation: Wang X, Cao J, Yan K, Liu D, Sun J. 2026. Control barrier function-based obstacle avoidance and formation cooperative control for multi-UAV system with unknown disturbance. *International Journal of Micro Air Vehicles* 18: e013 https://doi.org/10.48130/mav-0026-0014

Introduction

Owing to the advantages of fast flight speed and high robustness, the fixed-wing unmanned aerial vehicle (UAV) has gained widespread attention in various military and civilian fields[1,2]. Meanwhile, compared with a single UAV, the multiple UAV system (MUAVS) has obvious superiority in large-scale search and confrontation tasks, such as forest fire patrol, collaborative target tracking, and cooperative surveillance[3−5]. However, the safety control of MUAVS faces severe challenges and is worthy of long-term exploration.

Formation cooperative control is the primary problem to be solved for the safe flight of MUAVS, and a wide range of formation control approaches have been proposed in the existing literature. Guo et al.[6] and Yildiz et al.[7] developed the virtual structure-based formation control scheme for the UAV system to complete the tracking tasks with high quality. Peng et al.[8] and Duan et al.[9] proposed behavior-based methods to deal with the issues of dynamic task allocation and autonomous navigation, respectively. However, the virtual structure-based methods exhibit low fault tolerance and inflexibility. Meanwhile, the behavior-based methods struggle to ensure global performance. Consequently, this has driven the development of current consensus theory-based control technologies, with a considerable number of research outcomes having emerged. Shi et al.[10] focused on the asynchronous consensus issue in discrete-time heterogeneous MUAVS, considering the effects of dynamic communication topologies. In terms of formation safety, Wu et al.[11] put forward an improved consensus-based control algorithm to enhance the reliability of multi-UAV systems. By means of the multivariable adaptive control technique, Zhen et al.[12] designed a consensus-based flight controller for the MUAVS in the presence of unknown uncertainty. By integrating directional communications with consensus-based coordination, Dong et al.[13] constructed a distributed formation control framework for the multirotor UAV system. However, formation control is often coupled with autonomous obstacle avoidance, which poses new challenges to the task completion of UAV swarms.

Collision issues in the formation flight of MUAVS not only lead to mission failure but also cause property damage. Even worse, they may result in explosions and cause casualties. Therefore, various obstacle avoidance approaches have been proposed for the MUAVS in recent years, such as the rapidly exploring random tree method[14], particle swarm optimization method[15,16], and genetic algorithm[17,18]. However, the aforementioned methods consider the UAV as mass points, ignoring the dynamic characteristics of the system itself. In contrast, the control barrier function (CBF) method has attracted widespread attention by explicitly formulating obstacle avoidance constraints and integrating them into the control law design in real time[19]. Its essence lies in transforming obstacle avoidance from a path planning problem into a real-time control constraint problem, thus balancing system safety and task performance. Yin et al.[20] addressed the pursuit–evasion game issue of multi-UAVs by virtue of the enhanced CBF technique. Peng et al.[21] developed an innovative safe guidance method for the MUAVS in obstacle-rich environments by utilizing the high-order CBF. Ko & Chung[22] constructed a feasibility-guaranteed filter for the robotic systems to ensure operational safety based on the backup CBF method. Ma et al.[23] employed the discrete-time CBF for multi-rotor UAVs with limited sensory range to guarantee the robustness of the system during the learning and control stages. Moreover, the

https://doi.org/10.48130/mav-0026-0014

CBF approach is typically integrated with quadratic programming (QP), namely, the CBF-QP technique. Leveraging the optimization and solution capabilities of QP, a quantitative trade-off is achieved between 'satisfaction of safety constraints' and 'optimization of control performance', thereby significantly enhancing system performance. By means of the multiple Lyapunov functions method, Jang & Kim[24] developed a CBF-QP-based control scheme for mobile robots to guarantee safe tracking in complex environments. Hung et al.[25] designed a distributed tracking controller for MUAVS to achieve simultaneous occlusion and collision avoidance in light of the CBF-QP technique. Combining the CBF and QP methods, Yan et al.[26] presented an innovative iterative learning algorithm for a multi-agent system performing repetitive tasks to maintain the output safety of agents throughout every iteration. However, practical flight environments inevitably expose the MUAVS to unknown disturbances, which may degrade obstacle avoidance performance and even induce system instability.

To overcome this problem, many disturbance rejection schemes have been proposed over the past few decades, including the extended state observer (ESO)[27] and the disturbance observer[28]. However, the two aforementioned methods employ the estimated values for compensation after the observation error converges, while their control performance remains uncertain before the error converges. In contrast, the interval disturbance observer (IDO) can provide the upper and lower bounds of disturbance and encompass all possible values at any time, thereby guaranteeing its widespread application. Yong et al.[29] combined the IDO with the sliding mode control method for nonlinear systems to handle the problem of disturbance rejection. Luo et al.[30] proposed a distributed IDO for discrete-time multi-agent systems with unknown uncertainties to achieve coordination control. Wang et al.[31] developed a robust coordination control scheme for multi-agent systems based on the distributed IDO. In order to achieve safe formation flight, Ma et al.[32] presented an asymptotic consensus control strategy for the linear multi-agent systems based on the IDO method. Zhu et al.[33] introduced a set of IDOs for a quadrotor UAV with a cable-suspended load to enhance disturbance robustness and improve fault sensitivity. Yong et al.[34] explored the problem of tracking control for uncertain nonlinear systems under intense external disturbances to guarantee operational reliability. However, the coordinated control problem involving obstacle avoidance, formation maintenance, and anti-disturbance remains to be explored in depth.

Motivated by the above discussion, a CBF-QP-based cooperative formation control scheme with obstacle avoidance capability is designed for MUAVS under unknown disturbances. The main contributions are outlined below:

(1) Compared with the existing ESO and conventional disturbance observer methods, the proposed IDO provides real-time upper and lower bound estimations of the unknown disturbance. In this way, unknown disturbances can be enveloped at any time rather than only after the observation errors converge, which improves the disturbance rejection capability and safety performance of the MUAVS.

(2) Compared with the traditional obstacle avoidance methods that treat UAVs as mass points, the proposed CBF-QP-based method incorporates obstacle avoidance constraints into the real-time controller design, which achieves an effective trade-off between safe tracking performance and dynamic optimization.

(3) A robust formation obstacle avoidance control framework is developed by integrating IDO, consensus theory, and CBF-QP. The proposed control mechanism can not only meet the performance requirements for formation obstacle avoidance but also enhance the disturbance rejection capability of the entire MUAVS.

This paper is structured in the following manner. The section "Problem formulation and preparation" establishes the nonlinear dynamic model for fixed-wing MUAVS and introduces the necessary theoretical preliminaries. The detailed design procedure of the IDO and CBF-QP formation obstacle avoidance controller is elaborated in the section "Controller design and stability analysis". In the "Simulation results" section, the numerical simulation outcomes are presented to verify the effectiveness of the proposed control scheme. The section "Conclusions" summarizes the core findings and outlines future research prospects.

Notations: In this work, R_n and $R_{n\times m}$ denote the n-dimensional Euclidean space and the set of $n\times m$ matrices, and $R_+=\{x\in R: x\geq 0\}$. I_n denotes the $n\times n$ identity matrix. $diag\{c_1,\cdots,c_i\}$ represents the diagonal matrix with diagonal entries c_i. $\lambda_{\max}(\cdot)$ stands for the maximum eigenvalues. The symbol $\otimes$ denotes the Kronecker product, and $1_n\in R^{n\times 1}$ is the unit column vector.

Problem formulation and preparation

Graph theory

Consider a MUAVS consisting of n UAVs. The information exchange among them is described by the directed graph

$$G_r=(v_r,\varepsilon_r) \tag{1}$$

where $v_r=\{v_{r1},v_{r2},\ldots,v_{rn}\}$ is the node set, with each node corresponding to an individual UAV, and $\varepsilon_r=\{(v_{ri},v_{rj}): v_{ri},v_{rj}\in v_r\}$ is the edge set, indicating the direction of information transmission between UAVs. The topological structure is further characterized by the adjacency matrix $A_r=(a_{ij})\in R^{n\times n}$. Specifically, $a_{ij}=1$ if node j receives information from node i, and $a_{ij}=0$ otherwise. Self-loops are excluded, i.e., $a_{ii}=0$. The degree matrix is given by $D_r=diag\{d_{r1},\ldots,d_{rn}\}$, with $d_{ri}=\sum_{j=1}^{n}a_{ij}$. Consequently, the Laplacian matrix of G_r is defined as $L_r=D_r-A_r$.

For the leader-follower scenario, the augmented graph $\bar{G}_r=(\bar{v}_r,\bar{\varepsilon}_r)$ and the pinning matrix $S=diag\{s_1,\ldots,s_n\}$ are introduced, where $s_i=1$ if the i-th follower can access the leader's state, and $s_i=0$ otherwise.

CBF and QP

Definition 1[24]: A continuous function $\wp:[0,\alpha)\to[0,\infty)$ qualifies as a class K function for $\alpha>0$, if it is monotonically increasing and $\wp(0)=0$.

Definition 2[22,24]: Consider a control system as follows:

$$\dot{\eta}=f(\eta)+g(\eta)u \tag{2}$$

where $\eta\in R^n$ denotes the system state, $f:R^n\to R^n$ and $g:R^n\to R^{n\times q}$ are known nonlinear locally Lipschitz continuous functions, and $u\in R^q$ is the control input.

For a solution $\eta(t)$ of system (2), if the initial state satisfies $\eta(t_0)\in C\subset R^n$, it guarantees that $\eta(t)\in C$ holds for all $t\geq t_0$. Then, the set C is called the forward invariant set with respect to system (2).

Definition 3[22,23]: For a continuously differentiable function $\lambda:R^n\to R$, if there exists a class K function $\wp$ satisfying

$$\sup_{u\in U}[L_f\lambda(\eta)+L_g\lambda(\eta)u+\wp(\lambda(\eta))]\geq 0 \tag{3}$$

where U denotes the admissible set of control inputs, L_f and L_g represent the Lie derivative operators with respect to the vector fields $f(x)$ and $g(x)$, respectively. Then λ is called a CBF for system (2).

Based on Definition 2, the optimal controller for system (2) can be obtained by solving the following QP problem:

$$\begin{aligned} &u_{cbf} = \min_{u \in U} \|u\| \\ &s.t. L_f\lambda(\eta) + L_g\lambda(\eta)u \geq -\varphi(\lambda(\eta)) \end{aligned} \tag{4}$$

Problem description

For ease of presentation, the schematic illustration of the fixed-wing UAV structure is provided in Fig. 1, where χ, γ, and μ are the course yaw angle, course pitch angle, and course roll angle, respectively. (O_b, X_b, Y_b, Z_b) denotes the body frame and (O_g, X_g, Y_g, Z_g) refers to the inertial frame. Based on Newton's second law, a simplified dynamic model for any UAV within the formation in three-dimensional space can be described as[35]

$$\begin{aligned} \dot{x}_i &= V_i \cos\gamma_i \cos\chi_i \\ \dot{y}_i &= V_i \cos\gamma_i \sin\chi_i \\ \dot{z}_i &= V_i \sin\gamma_i \\ \dot{V}_i &= \frac{1}{m}(T_i - mg\sin\gamma_i) \\ \dot{\chi}_i &= \frac{1}{mV_i\cos\gamma_i} L_i \sin\mu_i \\ \dot{\gamma}_i &= \frac{1}{mV_i}(L_i\cos\mu_i - mg\cos\gamma_i) \end{aligned} \tag{5}$$

where m is the UAV mass and g the gravitational acceleration. For the ith fixed-wing UAV, its inertial position (x_i, y_i, z_i), speed V_i, heading angle χ_i, and flight-path angle γ_i constitute the state variables, while the lift L_i, thrust T_i, and course roll angle μ_i serve as the control inputs.

For simplifying the control design, we define an equivalent input vector $u_i = [u_{xi}, u_{yi}, u_{zi}]^T$ by setting $u_{xi} = T_i/(mg)$, $u_{yi} = L_i \sin\mu_i/(mg)$, and $u_{zi} = L_i\cos\mu_i/(mg)$. Evidently, the actual inputs L_i, T_i, μ_i are recoverable from the equivalent one u_i. When external disturbances are also accounted for, the dynamic model (5) of the ith fixed-wing UAV is rewritten as

$$\begin{aligned} \dot{\ell}_i &= \varsigma_i \\ \dot{\varsigma}_i &= F_i + G_i u_i + d_i \end{aligned} \tag{6}$$

where $\ell_i = [x_i, y_i, z_i]^T$ is the position vector, $d_i = [d_{ix}, d_{iy}, d_{iz}]^T$ represents the unknown disturbance, $\dot{\varsigma}_i = \ddot{\ell}_i = [\ddot{x}_i, \ddot{y}_i, \ddot{z}_i]^T$, $F_i = [0, 0, -g]^T$, and

$$G_i = \begin{bmatrix} g\cos\gamma_i\cos\chi_i & -g\sin\gamma_i & -g\cos\gamma_i\sin\chi_i \\ g\sin\gamma_i\cos\chi_i & g\cos\gamma_i & -g\sin\gamma_i\sin\chi_i \\ g\sin\chi_i & 0 & g\cos\chi_i \end{bmatrix} \tag{7}$$

Here, the unknown disturbance d_i is generated by the following exogenous system

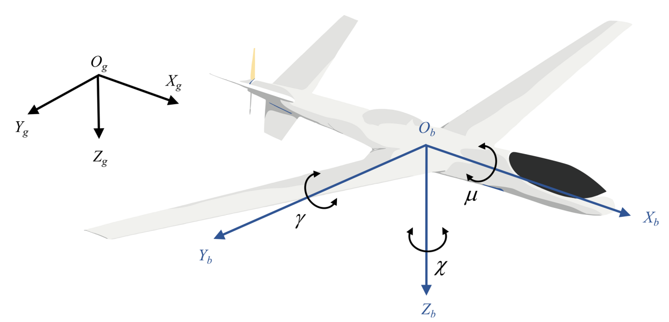

Fig. 1 The structure of fixed-wing UAV.

$$\begin{aligned} \dot{\delta}_i &= A_i\delta_i + B_i\varpi_i \\ d_i &= C_i\delta_i \end{aligned} \tag{8}$$

where $\delta_i \in R^{3\times1}$ is the state vector, $A_i \in R^{3\times3}$, $B_i \in R_+^{3\times1}$ and $C_i \in R_+^{3\times3}$ are the known constant matrices, ϖ_i denotes the unknown bounded input vectors satisfying $\varpi_i \leq \varpi_i^*$ with a known positive constant vector ϖ_i^*, $i = 1, 2, \cdots, N$.

This study focuses on the design of a formation control scheme with obstacle avoidance capability, which allows MUAVS to effectively reject disturbances while ensuring safe distances to obstacles. In light of this, several necessary assumptions and related lemmas are introduced.

Assumption 1[29,36]: For any $x \in R^n$, there exists a smooth nonlinear function $H(x): R^n \to R^m$ such that $\dfrac{\partial H(x)}{\partial x}$ exists.

Assumption 2[31]: Consider a directed graph G_r and its Laplacian $L_r \in R^{n\times n}$. When G_r has a directed spanning tree, the following hold: zero is a simple eigenvalue of L_r, the right eigenvector for this zero eigenvalue has only nonnegative entries, and every other eigenvalue has strictly positive real part.

Assumption 3[34,36]: The external disturbance d_i is unknown and bounded, satisfying $\|d_i\| \leq d_{im}$, where $d_{im} \in R_+$.

Assumption 4: In the cruise phase of the fixed-wing UAV, the sideslip angle and angle of attack are assumed to be zero. Meanwhile, the lateral force and drag can be safely ignored in the presence of the dominant lift force.

Lemma 1[31,34]: Consider the system $\dot{s}(t) = q_s s(t) + \omega_s(t)$ with $q_s \in R^{n\times n}$ being the state vector and $\omega_s(t) \in R_+^n$ being a time-varying vector. If q_s is a Metzler matrix for all $t \geq 0$, then the condition $q_s(t) \in R_+^n$ also holds for all $t \geq 0$.

Lemma 2[29]: Design a matrix $Q_s \in R^{n\times n}$ such that the matrix $(A_s - Q_s C_s)$ has same eigenvalue with a Metzler and Hurwitz matrix $H_s \in R^{n\times n}$, where $A_s, C_s \in R^{n\times n}$. If there exist two vectors $q_1 \in R^{1\times n}$ and $q_2 \in R^{1\times n}$ such that the pairs $(A_s - Q_s C_s, q_1)$ and (H_s, q_2) are observable, then $W_s^{-1} = O_{2s}^{-1} O_{1s}$ and $\Gamma_s = W_s^{-1} Q_s$, where

$$O_{1s} = \begin{bmatrix} q_1 \\ \vdots \\ q_1(A_s - Q_s C_s)^{n-1} \end{bmatrix}, O_{2s} = \begin{bmatrix} q_2 \\ \vdots \\ q_2 H_s^{\,n-1} \end{bmatrix}$$

Remark 1: For any smooth nonlinear functions, their partial derivatives always exist, so Assumption 1 is reasonable. Assumption 2 is a common assumption in the research of UAV swarm formation control and can be easily satisfied under practical UAV communication topologies. In practical systems, external disturbances always have bounded energy. Otherwise, no controller can suppress disturbances with infinite energy, which demonstrates the rationality of Assumption 3. During the cruise flight of fixed-wing UAVs, there is no sideslip of the airframe and the pitch angle is nearly horizontal. Meanwhile, the lateral force and drag force are far smaller than the lift force. Therefore, Assumption 4 is also reasonable. Assumptions 1–4 above are widely adopted in formation control and can be found in many existing literature[21,29,34,36].

Controller design and stability analysis

In this section, the proposed control scheme for MUAVS under unknown disturbances is formulated, which contains three core components: the IDO, the consensus-based formation control, and the CBF-QP-based obstacle avoidance strategy. For clearer illustration, the control flow block diagram of the proposed method is provided in Fig. 2.

https://doi.org/10.48130/mav-0026-0014

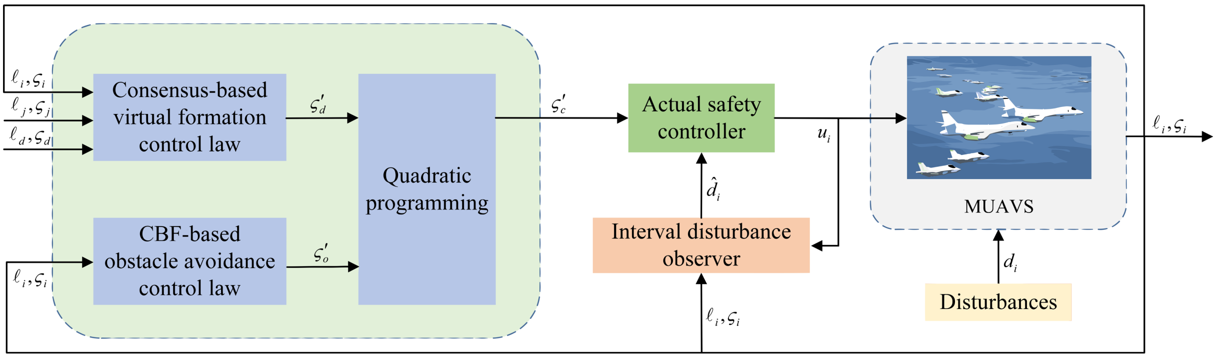

Fig. 2 Control flow block diagram of the proposed method.

The design of IDO

For the established affine nonlinear model (6) of MUAVS, the IDO designed in this subsection can effectively compensate for the impact of unknown disturbance. To facilitate the design of the IDO, an auxiliary variable $\psi_i \in R^{3\times 1}$ is introduced as[29]

$$\delta_i = W_i\psi_i + \vartheta(\varsigma_i) \tag{9}$$

$$\psi_i = W_i^{-1}\delta_i - W_i^{-1}\vartheta(\varsigma_i) \tag{10}$$

where $W_i \in R^{3\times 3}$ is a designed constant matrix, and $\vartheta(\varsigma_i)$ is a designed nonlinear function related to ς_i, $i = 1, 2, \cdots, N$.

Considering (6), (8) and (10), the derivative of ψ_i satisfies

$$\dot{\psi}_i = W_i^{-1}(A_i - \frac{\partial\vartheta(\varsigma_i)}{\partial\varsigma_i}C_i)W_i\psi_i + W_i^{-1}B_i\varpi_i + \Theta_i \tag{11}$$

where

$$\Theta_i = W_i^{-1}\left(A_i - \frac{\partial\vartheta(\varsigma_i)}{\partial\varsigma_i}C_i\right)\vartheta(\varsigma_i) - W_i^{-1}\frac{\partial\vartheta(\varsigma_i)}{\partial\varsigma_i}(G_iu_i + F_i) \tag{12}$$

Here, according to Assumption 1, the nonlinear function vector $\vartheta(\varsigma_i)$ can be designed as $\vartheta(\varsigma_i) = Q_i\varsigma_i$, which indicates that

$$\frac{\partial\vartheta(\varsigma_i)}{\partial\varsigma_i} = Q_i \tag{13}$$

where $Q_i \in R^{3\times 3}$ is a designed constant matrix.

Then the auxiliary variable can be expressed as

$$\dot{\psi}_i = W_i^{-1}(A_i - Q_iC_i)W_i\psi_i + W_i^{-1}B_i\varpi_i + \Theta_i \tag{14}$$

The IDO can be designed by estimating the upper boundary $\bar{\psi}_i$ and lower boundary $\underline{\psi}_i$ of the auxiliary variable, which is constructed as follows:

$$\dot{\bar{\psi}}_i = W_i^{-1}(A_i - Q_iC_i)W_i\bar{\psi}_i + W_i^{-1}B_i\varpi_i^* + \Theta_i \tag{15}$$

$$\dot{\underline{\psi}}_i = W_i^{-1}(A_i - Q_iC_i)W_i\underline{\psi}_i - W_i^{-1}B_i\varpi_i^* + \Theta_i \tag{16}$$

Define the estimation errors of the upper boundary as $\bar{z}_{\psi i} = \bar{\psi}_i - \psi_i$, and the estimation errors of the lower boundary as $\underline{z}_{\psi i} = \psi_i - \underline{\psi}_i$. Differentiating $\bar{z}_{\psi i}$ and $\underline{z}_{\psi i}$ and considering (15) and (16), we have

$$\dot{\bar{z}}_{\psi i} = W_i^{-1}(A_i - Q_iC_i)W_i\bar{z}_{\psi i} + \left|W_i^{-1}B_i\right|\varpi_i^* - W_i^{-1}B_i\varpi_i \tag{17}$$

$$\dot{\underline{z}}_{\psi i} = W_i^{-1}(A_i - Q_iC_i)W_i\underline{z}_{\psi i} + \left|W_i^{-1}B_i\right|\varpi_i^* + W_i^{-1}B_i\varpi_i \tag{18}$$

Remark 2: In this step, for a given vector $L = [l_1, \cdots, l_n]^T$, define $|L| = [|l_1|, \cdots, |l_n|]^T$. Taking (17) for example and assuming that $W_i^{-1}B_i = [l_{w1}, \cdots, l_{wn}]^T$, we have $\left|W_i^{-1}B_i\right| = [|l_{w1}|, \cdots, |l_{wn}|]^T$.

From the aforementioned analysis, the following theorem is derived:

Theorem 1: Consider the nonlinear system (6) under bounded disturbance given by (8). From the designed IDO (15) and (16), the intervals of the disturbance are given by

$$\bar{d}_i = C_i\left(\left(W_i^{-1}\right)^+\bar{\psi}_i - \left(W_i^{-1}\right)^-\underline{\psi}_i\right) + C_i\vartheta(\varsigma_i) \tag{19}$$

$$\underline{d}_i = C_i\left(\left(W_i^{-1}\right)^+\underline{\psi}_i - \left(W_i^{-1}\right)^-\bar{\psi}_i\right) + C_i\vartheta(\varsigma_i) \tag{20}$$

where $(W_i^{-1})^+ = \max(W_i^{-1}, O)$ and $(W_i^{-1})^- = (W_i^{-1})^+ - (W_i^{-1})$ with O being the zero matrix.

Furthermore, if the matrix $W_i^{-1}(A_i - Q_iC_i)W_i$ is Hurwitz and Metzler, and the boundary estimation errors $\bar{z}_{di} = \bar{d}_i - d_i$ and $\underline{z}_{di} = d_i - \underline{d}_i$ are always nonnegative and bounded, and the initial conditions that $\bar{z}_{\psi i}(0)$ and $\underline{z}_{\psi i}(0)$ are nonnegative.

Proof: The dynamics of boundary estimation errors $\dot{\bar{z}}_{\psi i}$ and $\dot{\underline{z}}_{\psi i}$ can be written as

$$\dot{\bar{z}}_{\psi i} = H_i\bar{z}_{\psi i} + \bar{\Psi}_i \tag{21}$$

$$\dot{\underline{z}}_{\psi i} = H_i\underline{z}_{\psi i} + \underline{\Psi}_i \tag{22}$$

where $H_i = W_i^{-1}(A_i - Q_iC_i)W_i$, $\bar{\Psi}_i = \left|W_i^{-1}B_i\right|\varpi_i^* - W_i^{-1}B_i\varpi_i$ and $\underline{\Psi}_i = \left|W_i^{-1}B_i\right|\varpi_i^* + W_i^{-1}B_i\varpi_i$.

According to Lemma 1, an appropriate matrix is chosen such that $H_i = W_i^{-1}(A_i - Q_iC_i)W_i$ is Hurwitz. Namely, the following equation holds:

$$H_i^TE_i + E_iH_i = -K_i \tag{23}$$

where K_i and E_i are the positive definite matrix.

Select the Lyapunov function V_1 as

$$V_1 = \bar{z}_{\psi i}^TE_i\bar{z}_{\psi i} + \underline{z}_{\psi i}^TE_i\underline{z}_{\psi i} \tag{24}$$

By invoking (21) and (22), taking the time derivative of V_1 yields

$$\begin{aligned}
\dot{V}_1 &= \dot{\bar{z}}_{\psi i}^TE_i\bar{z}_{\psi i} + \bar{z}_{\psi i}^TE_i\dot{\bar{z}}_{\psi i} + \dot{\underline{z}}_{\psi i}^TE_i\underline{z}_{\psi i} + \underline{z}_{\psi i}^TE_i\dot{\underline{z}}_{\psi i} \\
&= \left(H_i\bar{z}_{\psi i} + \bar{\Psi}_i\right)^TE_i\bar{z}_{\psi i} + \bar{z}_{\psi i}^TE_i\left(H_i\bar{z}_{\psi i} + \bar{\Psi}_i\right) \\
&\quad + \left(H_i\underline{z}_{\psi i} + \underline{\Psi}_i\right)^TE_i\underline{z}_{\psi i} + \underline{z}_{\psi i}^TE_i\left(H_i\underline{z}_{\psi i} + \underline{\Psi}_i\right) \\
&= -\bar{z}_{\psi i}^TK_i\bar{z}_{\psi i} - \underline{z}_{\psi i}^TK_i\underline{z}_{\psi i} + 2\bar{\Psi}_i^TE_i\bar{z}_{\psi i} + 2\underline{\Psi}_i^TE_i\underline{z}_{\psi i} \\
&\le -\bar{z}_{\psi i}^TK_i\bar{z}_{\psi i} - \underline{z}_{\psi i}^TK_i\underline{z}_{\psi i} + 2\left\|\bar{\Psi}_i^TE_i\right\|\left\|\bar{z}_{\psi i}\right\| + 2\left\|\underline{\Psi}_i^TE_i\right\|\left\|\underline{z}_{\psi i}\right\| \\
&\le -\bar{z}_{\psi i}^T(K_i - I_i)\bar{z}_{\psi i} - \underline{z}_{\psi i}^T(K_i - I_i)\underline{z}_{\psi i} + \bar{\lambda}_{di}^2 + \underline{\lambda}_{di}^2
\end{aligned} \tag{25}$$

where $\left\|\bar{\Psi}_i^TE_i\right\| \le \bar{\lambda}_{di}$ and $\left\|\underline{\Psi}_i^TE_i\right\| \le \underline{\lambda}_{di}$.

Considering (21) and (22), the disturbance estimation errors can be further written in the following form:

$$\bar{z}_{di} = C_i\left(\Phi_i^+\bar{\psi}_i - \Phi_i^-\underline{\psi}_i - \Phi_i\psi_i\right) = C_i\Phi_i^+\bar{z}_{\psi i} + C_i\Phi_i^-\underline{z}_{\psi i}, \tag{26}$$

$$\underline{z}_{di} = C_i\left(\Phi_i^- \bar{\psi}_i - \Phi_i^+ \underline{\psi}_i + \Phi_i \psi_i\right) = C_i \Phi_i^- \bar{z}_{\psi i} + C_i \Phi_i^+ \underline{z}_{\psi i} \tag{27}$$

where $\Phi_i = \Phi_i^+ - \Phi_i^-$, since $C_i \geq 0$, $\Phi_i^+ \geq 0$, $\Phi_i^- \geq 0$, $\bar{z}_{\psi i}$ and $\underline{z}_{\psi i}$ are non-negative and bounded, the disturbance estimation errors $\bar{z}_{di}$ and $\underline{z}_{di}$ are non-negative and bounded, that is, the true disturbance d_i satisfies $\underline{d}_i \leq d_i \leq \bar{d}_i$.

In this step, the key lies in selecting adequate matrices such that H_i is Metzler and Hurwitz stable. According to Lemma 2, H_i can be computed by solving a Sylvester equation: $W_i^{-1}A_i - H_i W_i^{-1} = \Gamma_i C_i$, $\Gamma_i = W_i^{-1} Q_i$, where H_i and A_i share the same eigenvalue[37].

Remark 3: Since the estimation errors $\bar{z}_{di}$ and $\underline{z}_{di}$ are always nonnegative and bounded in Theorem 1, we can obtain that $z_{di}^* = \bar{z}_{di} + \underline{z}_{di} = \bar{d}_i - \underline{d}_i$ is also bounded. Applying the inequality condition, it follows that $-\frac{1}{2}(\bar{d}_i - \underline{d}_i) \leq d_i - \hat{d}_i \leq \frac{1}{2}(\bar{d}_i - \underline{d}_i)$, which means that $z_{di} = d_i - \hat{d}_i$ is bounded, $i = 1, 2, \cdots, N$.

Consensus-based virtual formation control design

The tracking position error $z_{\ell i}$ and velocity error $z_{\varsigma i}$ of the ith follower UAV are defined as[38]

$$z_{\ell i} = \sum_{j=1}^{N} a_{ij}\left(\ell_i - \kappa_{ij} - \ell_j\right) + s_i(\ell_i - \kappa_i - \ell_d) \tag{28}$$

$$z_{\varsigma i} = \sum_{j=1}^{N} a_{ij}\left(\varsigma_i - \varsigma_j\right) + s_i(\varsigma_i - \varsigma_d) \tag{29}$$

where $z_{\ell i} = [z_{\ell ix}, z_{\ell iy}, z_{\ell iz}]^T$ and $z_{\varsigma i} = [z_{\varsigma ix}, z_{\varsigma iy}, z_{\varsigma iz}]^T$ represent the position error and velocity error of the ith UAV in the three-axis directions, respectively. a_{ij} and s_i are the adjacency weight among followers and the pinning weight from the leader. $\kappa_{ij} = \kappa_{id} - \kappa_{jd}$ is the desired offset between the iUAV and jUAV with $\kappa_{id} = \ell_i - \ell_d$ and $\kappa_{jd} = \ell_j - \ell_d$, ℓ_i and ς_i are the position and velocity of the ith follower UAV, ℓ_d and ς_d are those of the leader UAV.

Applying algebraic operations to (28) and (29) yields

$$z_\ell = L_\ell(\ell - \kappa - \ell_d') \tag{30}$$

$$z_\varsigma = L_\ell(\varsigma - \varsigma_d') \tag{31}$$

where $L_\ell = (L_r + S) \otimes I_3$, $L_r \in R^{n \times n}$ denotes the follower sub-graph Laplace matrix, $S = diag\{s_1, \cdots s_i\}$ is the leader-follower communication weight matrix with $s_i > 0$. Since L_r is positive semi-definite and S is a positive diagonal matrix with at least one positive entry, $(L_r + S)$ is positive definite and thus invertible, which implies the invertibility of L_ℓ. $z_\ell = [z_{\ell 1}, \ldots, z_{\ell i}]^T$, $z_\varsigma = [z_{\varsigma 1}, \ldots, z_{\varsigma i}]^T$, $\ell = [\ell_1, \cdots, \ell_i]^T$, $\varsigma = [\varsigma_1, \cdots, \varsigma_i]^T$, $\kappa = [\kappa_1, \ldots, \kappa_i]^T$, $\ell_d' = 1_n \otimes \ell_d$, $\varsigma_d' = 1_n \otimes \varsigma_d$, $i = 1, 2, \cdots, N$.

Taking the derivative of z_ℓ produces

$$\dot{z}_\ell = L_\ell(\dot{\ell} - \dot{\ell}_d') = L_\ell(L_\ell^{-1} z_\varsigma + \varsigma_d' - \dot{\ell}_d') \tag{32}$$

Design virtual formation control input as

$$\varsigma_d' = -L_\ell^{-1} \lambda_\ell z_\ell + \dot{\ell}_d' \tag{33}$$

where $\lambda_\ell = diag\{\lambda_{\ell 1}, \cdots, \lambda_{\ell i}\}$ is the designed positive definite matrix, and $\lambda_{\ell i} = diag\{\lambda_{\ell ix}, \lambda_{\ell iy}, \lambda_{\ell iz}\}$, $i = 1, 2, \cdots, N$.

By substituting (33) into (32), we obtain

$$\dot{z}_\ell = -\lambda_\ell z_\ell + z_\varsigma \tag{34}$$

Subsequently, the Lyapunov function candidate is selected as

$$V_2 = \frac{1}{2} z_\ell^T z_\ell \tag{35}$$

Invoking (34), we have

$$\dot{V}_2 = z_\ell^T \dot{z}_\ell = z_\ell^T z_\varsigma - z_\ell^T \lambda_\ell z_\ell \tag{36}$$

CBF-QP-based obstacle avoidance and formation cooperative control design

The function of CBF is to guarantee a safety margin between the position of the UAVs and obstacles. To avoid collision avoidance between the UAVs and obstacles, the safety set C_{bi} for the ith UAV is defined as

$$C_{bi} = \left\{\ell_i \in R^{3 \times 1} \,|\, h_i(\ell) \geq 0\right\} \tag{37}$$

where $h_i(\ell)$ is regarded as a CBF for the ith UAV with the form of[20]

$$h_i(\ell) = (\ell_i - \ell_{oi})^T(\ell_i - \ell_{oi}) - d_{safe}^2 \tag{38}$$

where $\ell_{oi} = [\ell_{oix}, \ell_{oiy}, \ell_{oiz}]^T$ represents the three-axis positions of multiple obstacles, and d_{safe} represents the safe distance of the avoidance area.

Design $h(\ell) = [h_1(\ell), \cdots, h_i(\ell)]^T$ as the CBF of the entire MUAVS. Clearly, it can be further expressed as

$$h(\ell) = \begin{bmatrix} h_1(\ell) \\ \vdots \\ h_i(\ell) \end{bmatrix} = \begin{bmatrix} (\ell_1 - \ell_{o1})^T(\ell_1 - \ell_{o1}) \\ \vdots \\ (\ell_i - \ell_{oi})^T(\ell_i - \ell_{oi}) \end{bmatrix} - d_{safe}^2 1_n \tag{39}$$

Based on (6), the time derivative of (39) can be obtained as

$$\dot{h}(\ell) = \begin{bmatrix} \dot{h}_1(\ell) \\ \vdots \\ \dot{h}_i(\ell) \end{bmatrix} = 2L^o \varsigma \tag{40}$$

where $L^o = diag\left\{(\ell_1 - \ell_{o1})^T, \cdots, (\ell_i - \ell_{oi})^T\right\}$.

The core function of QP is to efficiently solve for the optimal control input that meets the obstacle avoidance requirements under the safety constraints provided by the CBF, while balancing the UAV's mission objectives and dynamic constraints. Combining CBF and QP, the virtual safety control law ς_c is defined as

$$\begin{aligned} \varsigma_c &= \min_{\varsigma} \left\|\varsigma - \varsigma_d'\right\|^2 \\ &s.t.\ \dot{h}(\ell) \geq 0 \end{aligned} \tag{41}$$

where $\varsigma_c = [\varsigma_{c1}, \cdots, \varsigma_{ci}]^T$.

Remark 4: Here, each $\dot{h}_i(\ell) \geq 0$ serves as the constraint condition for $\min_{\varsigma_i} \left\|\varsigma_i - \varsigma_{di}'\right\|^2$, where ς_{di}' is the i^{th} element of ς_d'. Then, the virtual safety control law ς_{ci} for each UAV can be derived. Therefore, for the whole MUAVS consisting of i UAVs, the resulting virtual safety control law is $\varsigma_c = [\varsigma_{c1}, \cdots, \varsigma_{ci}]^T$.

Define the error between the virtual safety control law ς_c and the virtual formation control law ς_d' as $z_c = \varsigma_c - \varsigma_d'$. In this work, the error z_c and its first-order derivative are assumed to be bounded, namely, there exist positive constants making $\|z_c\| \leq \delta_c$ and $\|\dot{z}_c\| \leq \delta_\Theta$ hold[19].

Remark 5: The boundedness assumptions for the error between the virtual safety control law ς_c and the virtual formation control law ς_d', as well as its time derivative, are reasonable and well-founded. The CBF-QP constraint confines the system state to the predefined safe set, ensuring the boundedness of ς_c. Combined with the boundedness of ς_d' and its derivatives, the error and its derivative are consequently bounded. Such assumptions are common and acceptable in the stability analysis of constrained formation control systems.

Differentiating z_ς yields

$$\dot{z}_\varsigma = L_\ell(F + Gu + d - \dot{\varsigma}_d') \tag{42}$$

where $F = [F_1, \cdots, F_i]^T$, $G = diag\{G_1, \cdots, G_i\}$, $u = [u_1, \cdots, u_i]^T$, $d = [d_1, \cdots, d_i]^T$, $i = 1, 2, \cdots, N$.

https://doi.org/10.48130/mav-0026-0014

Invoking (41) and (42), the resulting obstacle avoidance and formation cooperative controller is designed below:

$$u = G^{-1}[L_\ell^{-1}(-z_\ell - \lambda_\varsigma z_\varsigma) - F - \hat{d} + \dot{\varsigma}_c] \tag{43}$$

where $\lambda_\varsigma = diag\{\lambda_{\varsigma 1}, \cdots, \lambda_{\varsigma i}\} > 0$, and $\lambda_{\varsigma i} = diag\{\lambda_{\varsigma ix}, \lambda_{\varsigma iy}, \lambda_{\varsigma iz}\}$, $\hat{d} = [\hat{d}_1, \ldots, \hat{d}_i]^T$, $\hat{d}_i = \frac{1}{2}(\bar{d}_i + \underline{d}_i)$ is the disturbance estimation value, $i = 1, 2, \cdots, N$.

By substituting (43) into (42), we obtain

$$\dot{z}_\varsigma = -\lambda_\varsigma z_\varsigma - z_\ell - \hat{d} + \dot{\varsigma}_c + d - \dot{\varsigma}'_d \tag{44}$$

Choose the Lyapunov candidate function V_3 as

$$V_3 = \frac{1}{2} z_\ell^T z_\ell + \frac{1}{2} z_\varsigma^T z_\varsigma \tag{45}$$

Considering (34) and (44), it gives

$$\begin{aligned}
\dot{V}_3 &= z_\ell^T \dot{z}_\ell + z_\varsigma^T \dot{z}_\varsigma \\
&= z_\ell^T(-\lambda_\ell z_\ell + z_\varsigma) + z_\varsigma^T(-\lambda_\varsigma z_\varsigma - z_\ell - \hat{d} + \dot{\varsigma}_c + d - \dot{\varsigma}'_d) \\
&= -z_\ell^T \lambda_\ell z_\ell - z_\varsigma^T \lambda_\varsigma z_\varsigma + z_\varsigma^T \dot{z}_c + z_\varsigma^T z_d \\
&\le -z_\ell^T \lambda_\ell z_\ell - z_\varsigma^T \lambda_\varsigma z_\varsigma + \frac{1}{2}(z_\varsigma^T z_\varsigma + \dot{z}_c^T \dot{z}_c) + \frac{1}{2}(z_\varsigma^T z_\varsigma + z_d^T z_d) \\
&\le -z_\ell^T \lambda_\ell z_\ell - z_\varsigma^T \bar{\lambda}_\varsigma z_\varsigma + \frac{1}{2} \dot{z}_c^T \dot{z}_c + \frac{1}{2} z_d^T z_d \\
&\le -z_\ell^T \lambda_\ell z_\ell - z_\varsigma^T \bar{\lambda}_\varsigma z_\varsigma + \frac{1}{2}\delta_\Theta^2 + \frac{1}{2}\delta_d^2
\end{aligned} \tag{46}$$

where $z_d = [z_{d1}, \cdots, z_{di}]^T$ is the bounded estimation errors, $||\dot{z}_c|| \le \delta_\Theta$, $||z_d|| \le \delta_d$, where δ_Θ, δ_d are positive constants, $\bar{\lambda}_\varsigma = \lambda_\varsigma - I$, $I \in R^{3n \times 3n}$, $i = 1, 2, \cdots, N$.

According to the definition of the controller in dynamic system (6), the actual control inputs are obtained as follows:

$$\begin{aligned}
T_i &= u_{xi} mg \\
\mu_i &= \arctan\left(\frac{u_{yi}}{u_{zi}}\right) \\
L_i &= \frac{u_{yi} mg}{\sin \mu_i}
\end{aligned} \tag{47}$$

Stability analysis

Overall, the above analysis can be stated as the following theorem:

Theorem 2: For the nonlinear model (6) of MUAVS with unknown disturbance, the IDO is designed as (15) and (16). Under the proposed safe formation and obstacle avoidance flight controller (43), all error signals of the whole MUAVS are ultimately uniformly bounded, and the follower UAV can effectively track the leader UAV.

Proof: Let $V_4 = V_1 + V_3$ be a Lyapunov candidate. Then, differentiating it and applying (25) and (46) yields

$$\begin{aligned}
\dot{V}_4 &= \dot{V}_1 + \dot{V}_3 \\
&\le -\bar{z}_{\psi i}^T (K_i - I_i) \bar{z}_{\psi i} - \underline{z}_{\psi i}^T (K_i - I_i) \underline{z}_{\psi i} + \bar{\lambda}_{di}^2 \\
&\quad + \underline{\lambda}_{di}^2 - z_\ell^T \lambda_\ell z_\ell - z_\varsigma^T \bar{\lambda}_\varsigma z_\varsigma + \frac{1}{2}\delta_\Theta^2 + \frac{1}{2}\delta_d^2 \\
&\le -\varepsilon_0 V_4 + \varepsilon_1
\end{aligned} \tag{48}$$

where $\varepsilon_0 = \min\left\{\frac{K_i - I_i}{\lambda_{\max} E_i}, 2\lambda_\ell, 2\bar{\lambda}_\varsigma\right\}$, $\varepsilon_1 = \bar{\lambda}_{di}^2 + \underline{\lambda}_{di}^2 + \frac{1}{2}\delta_\Theta^2 + \frac{1}{2}\delta_d^2$.

Integration of (48) produces

$$0 \le V_4 \le \frac{\varepsilon_1}{\varepsilon_0} + \left[V_4(0) - \frac{\varepsilon_1}{\varepsilon_0}\right] e^{-\varepsilon_0 t} \tag{49}$$

According to (49), V_4 gradually converges as time goes on, which indicates that all error signals in the closed-loop system are ultimately uniformly bounded. This concludes the proof.

Remark 6: The stability of the system is further enhanced by the synergistic operation of the IDO and CBF-QP. The disturbance compensation provided by the IDO enables the CBF-QP-based controller to accurately account for external disturbance in real time. This synergy guarantees robust safety against obstacles while optimizing the tracking performance.

Remark 7: In this section, the IDO technique is combined with the CBF-QP method to realize formation control with obstacle avoidance and disturbance rejection. In practice, external disturbances will cause position and velocity deviations of UAVs and make the actual flight trajectories deviate significantly from the preset trajectories. On one hand, these adverse effects will greatly reduce the safety margin of obstacle avoidance, which may easily lead to collisions between UAVs or between UAVs and obstacles. On the other hand, persistent disturbances will violate the predefined relative position constraints of the formation, resulting in formation dispersion and failure of cooperative tasks. Therefore, the integration of the IDO and CBF-QP technologies lays a solid foundation for the safe flight of UAV formations under disturbances.

Simulation results

For validation purposes, a formation of one leader UAV and four followers is adopted, where the follower UAVs maintain a rectangular geometry relative to the leader. The communication topology of the leader-follower MUAVS is depicted in Fig. 3, where UAV_0 denotes the leader UAV and UAV_1–UAV_4 denotes the follower UAVs. The directed edges represent the information flow among UAVs. Considering the definitions in (1), the matrixes A_r, D_r, L_r and S are chosen as

$$A_r = \begin{bmatrix} 0 & 1 & 1 & 0 \\ 1 & 0 & 0 & 1 \\ 1 & 0 & 0 & 1 \\ 0 & 1 & 1 & 0 \end{bmatrix}, D_r = \begin{bmatrix} 2 & 0 & 0 & 0 \\ 0 & 2 & 0 & 0 \\ 0 & 0 & 2 & 0 \\ 0 & 0 & 0 & 2 \end{bmatrix},$$

$$L_r = \begin{bmatrix} 2 & -1 & -1 & 0 \\ -1 & 2 & 0 & -1 \\ -1 & 0 & 2 & -1 \\ 0 & -1 & -1 & 2 \end{bmatrix}, S = \begin{bmatrix} 1 & 0 & 0 & 0 \\ 0 & 0 & 0 & 0 \\ 0 & 0 & 0 & 0 \\ 0 & 0 & 0 & 0 \end{bmatrix}$$

The reference position of the leader UAV is $\ell_d = [0.1t^2, 0.1t^2, 0.1t^2]$, the parameters of each follower UAV are $\lambda_{\ell i} = diag\{3,3,8\}$, $\lambda_{\varsigma i} = diag\{5,5,7\}$, i = 1, 2, 3, 4. Their relative positions are illustrated in Table 1.

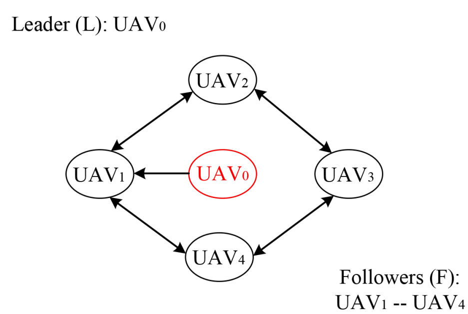

Fig. 3 MUAVS communication topology schematic diagram.

Table 1. Relative position between UAV_i and UAV_0.

Number	X	Y	Z
UAV_1	0	3	5
UAV_2	0	−3	5
UAV_3	0	3	−5
UAV_4	0	−3	−5

According to (8), the parameters of the exogenous system is given as

$$A_i = \begin{bmatrix} 0 & 1 & 0 \\ -1 & 0 & 0 \\ 0 & -1 & 0 \end{bmatrix}, B_i = \begin{bmatrix} 0 \\ 2 \\ 0 \end{bmatrix}, C_i = \begin{bmatrix} 1 & 0 & 0 \\ 0 & 1 & 0 \\ 0 & 0 & 1 \end{bmatrix}, i = 1,2,3,4$$

The other control design parameters are chosen as

$$W_i = \begin{bmatrix} 30 & 4 & 0 \\ -20 & 12 & 0 \\ 0 & -12 & 50 \end{bmatrix}, \varpi_i = \sin(0.5\pi t), \varpi_i^* = 2, i = 1,2,3,4$$

$$Q_1 = \begin{bmatrix} 30 & 4 & 0 \\ -20 & 12 & 0 \\ 0 & -12 & 50 \end{bmatrix}, Q_2 = \begin{bmatrix} 14 & 3 & 0 \\ -18 & 3 & 0 \\ 0 & -10 & 10 \end{bmatrix},$$

$$Q_3 = \begin{bmatrix} 40 & 3 & 0 \\ -1 & 9 & 0 \\ 0 & -10 & 20 \end{bmatrix}, Q_4 = \begin{bmatrix} 7 & 3 & 0 \\ -9 & 9 & 0 \\ 0 & -10 & 25 \end{bmatrix}$$

The simulation results are displayed in Figs 4–11. Figure 4 exhibits the disturbance estimation, where orange and green dashed lines represent the estimated upper and lower bounds, while the black solid lines are the actual disturbance values. Simulation results demonstrate that the designed IDO can cover the disturbance estimate at any time, rather than only after the estimation error has

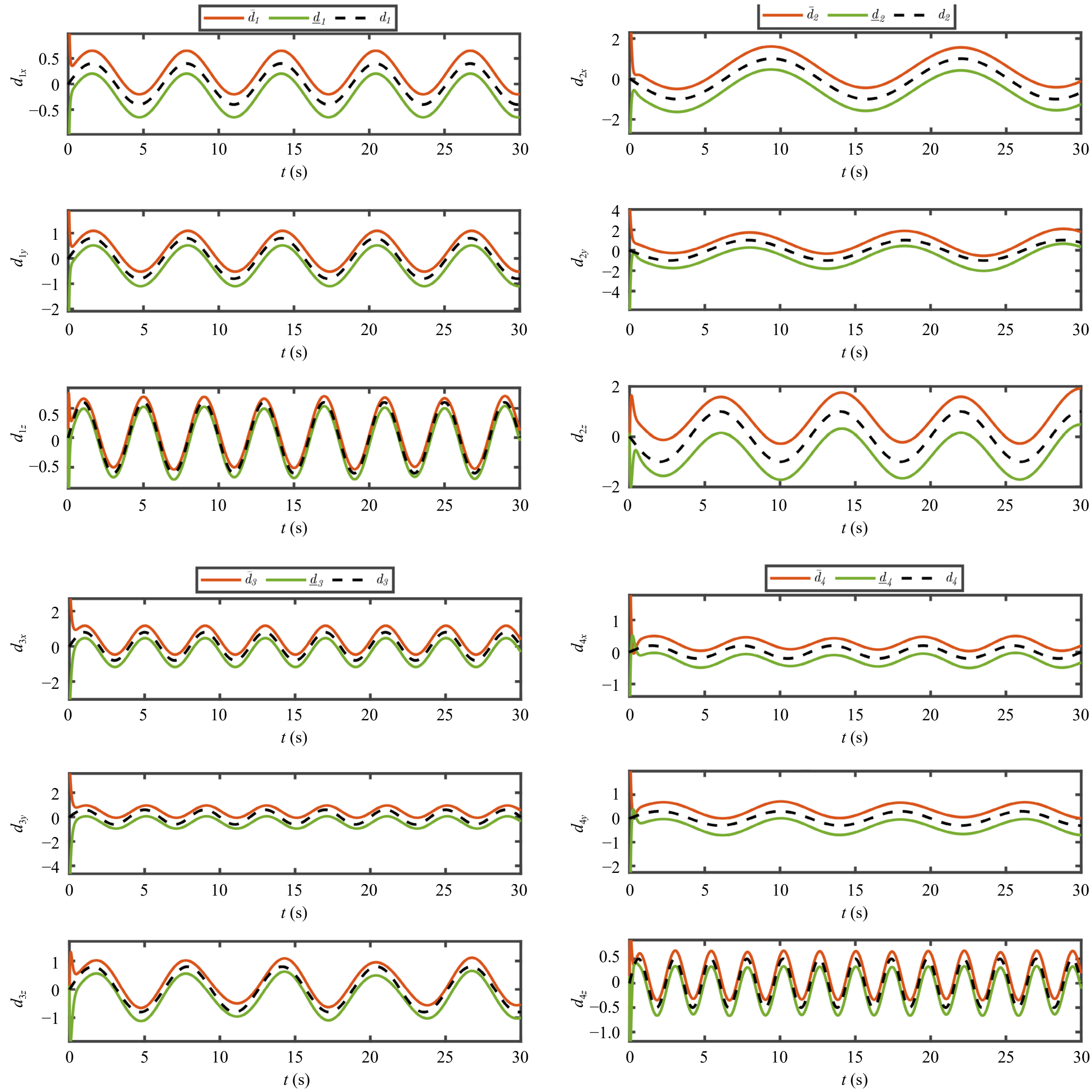

Fig. 4 Estimation results of unknown disturbance under the IDO.

https://doi.org/10.48130/mav-0026-0014

converged. This also implies an improved disturbance rejection capability of the MUAVS throughout the entire process.

Moreover, comparative simulations are performed to validate the superiority of the designed IDO compared with the traditional ESO. The mean value of the upper and lower bounds of the IDO is adopted as the disturbance estimation. Figure 5 presents these comparative results, where the black dashed line represents the actual disturbance, the blue dashed line denotes the estimated result of the ESO, and the orange dashed line is that under the proposed IDO. As evident from Fig. 5, both the IDO and ESO methods are capable of accurately estimating unknown disturbances. However, unlike the ESO, which requires a finite convergence time to asymptotically track the disturbance, the proposed IDO provides mathematically guaranteed upper and lower bounds from the very initial moment. Furthermore, the IDO achieves smaller overshoot and a faster transient response.

Meanwhile, to verify the feasibility and advantage of the proposed CBF-based obstacle avoidance strategy, comparative simulations against the conventional artificial potential field (APF) method are performed. In the APF paradigm, the destination generates an attractive potential acting on the UAV, while each obstacle produces a repulsive potential. The resultant force is the vector superposition of the attractive force from the destination and the repulsive forces from all obstacles, and the UAV reaches the target when its potential energy drops to zero. It is well recognized, however, that the APF approach suffers from intrinsic limitations, notably the goal non-reachability and local minima issues.

To illustrate the non-reachability problem, we place an obstacle near the target at coordinates (100,100,100), as detailed in Table 2. This obstacle, denoted as Obstacle_5, lies closest to the destination and falls within the attractive influence region of the UAV_1. As a result, when the UAV approaches the target, the repulsive force

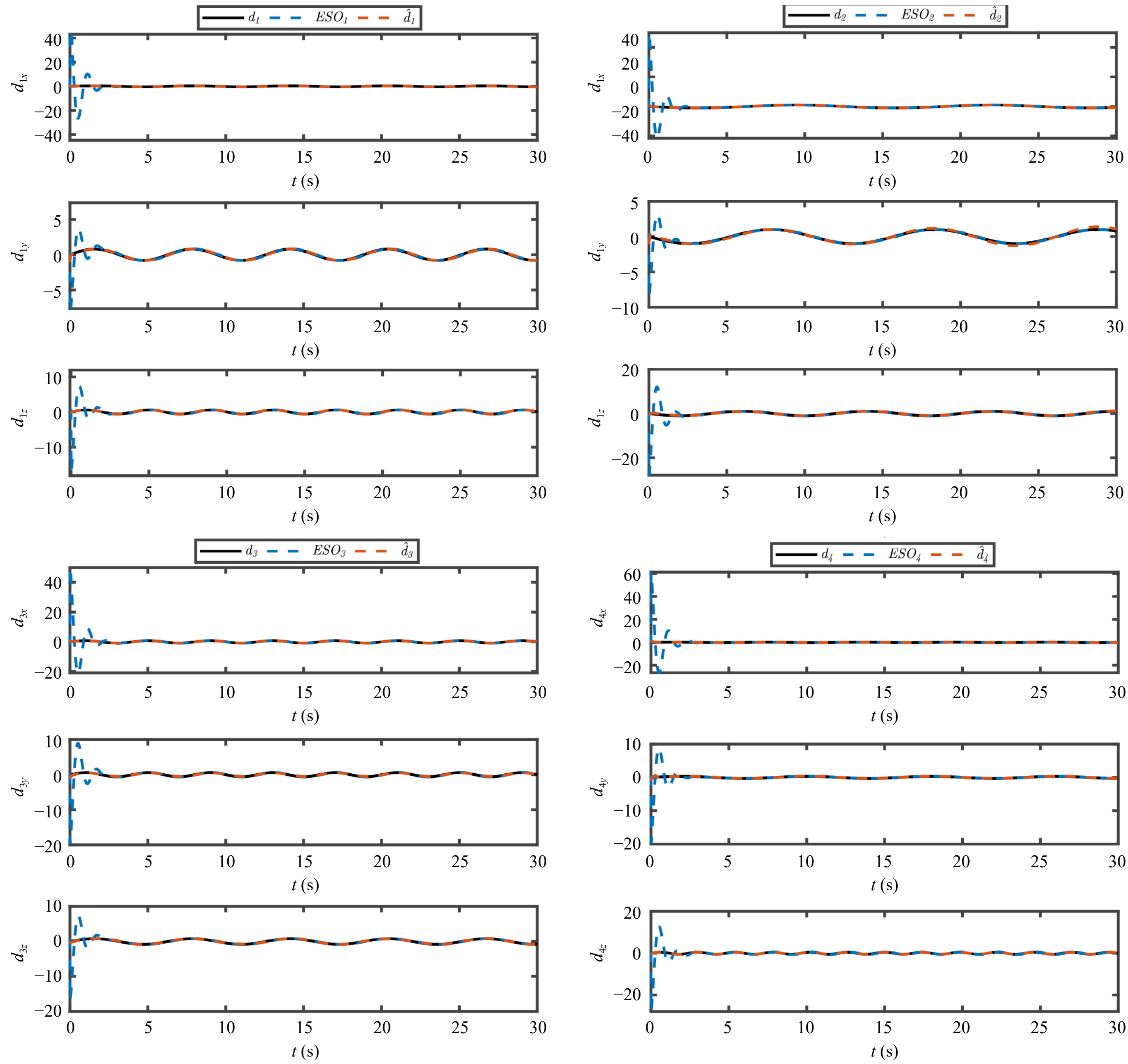

Fig. 5 Comparison of estimation results of unknown disturbance under the IDO and ESO.

Table 2. Parameter setting of the obstacles.

Number	Obstacle position	Obstacle radius
Obstacle_1	(30, 50, 41)	7
Obstacle_2	(45, 30, 35)	9
Obstacle_3	(50, 60, 45)	8
Obstacle_4	(70, 55, 75)	12
Obstacle_5	(80, 83, 85)	5

from the obstacle overwhelms the attractive force from the destination, leading to the well-known goal non-reachability phenomenon. As shown in Fig. 6, the UAV undergoes persistent oscillations in the vicinity of the target and ultimately fails to land on the desired point. By contrast, Fig. 7 reveals that under the proposed CBF-imposed constraints, the UAV reaches the target smoothly. These comparative results clearly demonstrate that the CBF method effectively overcomes the goal non-reachability defect inherent in the APF scheme.

The three-axis tracking trajectories and corresponding errors for UAV_3 and UAV_4 are depicted in Figs 8 and 9, where the dashed black line indicates the reference, and the orange and blue solid lines correspond to the CBF and APF schemes, respectively. Although both methods ensure collision-free navigation, CBF-QP yields less conservative safety adjustments, leading to shorter avoidance routes and tighter tracking with reduced position errors, as it formulates safety constraints in a mathematically optimized manner. With dynamically allocated control priority, formation control takes precedence in safe regions, whereas CBF-QP activates and enforces safety constraints upon obstacle proximity to guarantee strict safety distance margins.

This is further supported by the quantitative comparison in Tables 3 and 4, which list the MAE and RMSE for UAV_3 and UAV_4 during the obstacle-avoidance phase. The data consistently show that CBF offers smaller tracking errors and RMSE across most scenarios, along with more economical flight paths.

Figure 10 demonstrates the motion trajectories in three-dimensional coordinates under the CBF method, confirming that the formation reaches the predefined configuration within 5 s.

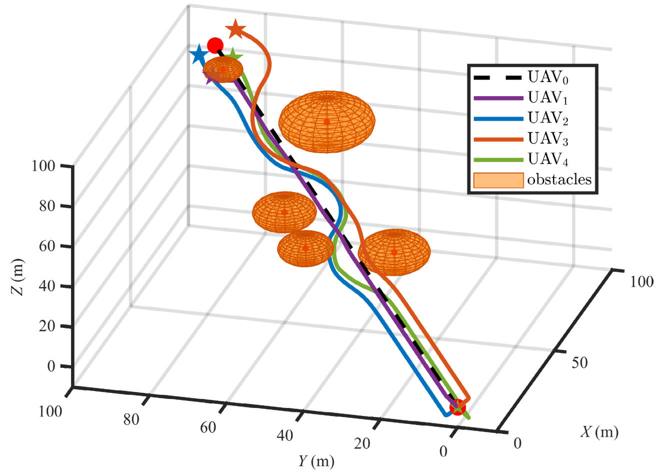

Fig. 6 3D diagram of APF-based rectangular formation obstacle avoidance.

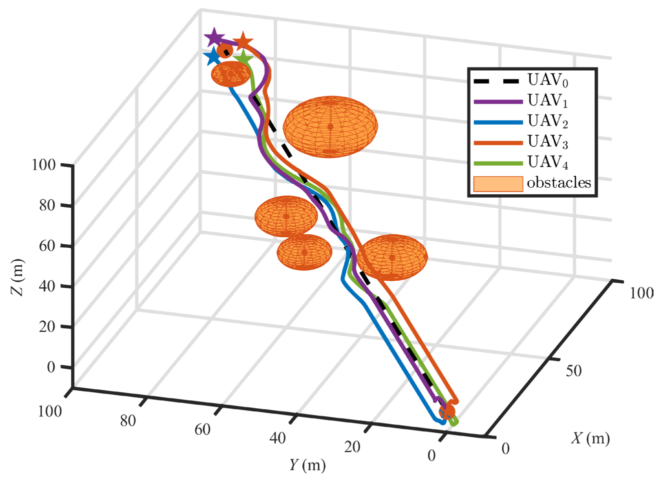

Fig. 7 3D diagram of CBF-based rectangular formation obstacle avoidance.

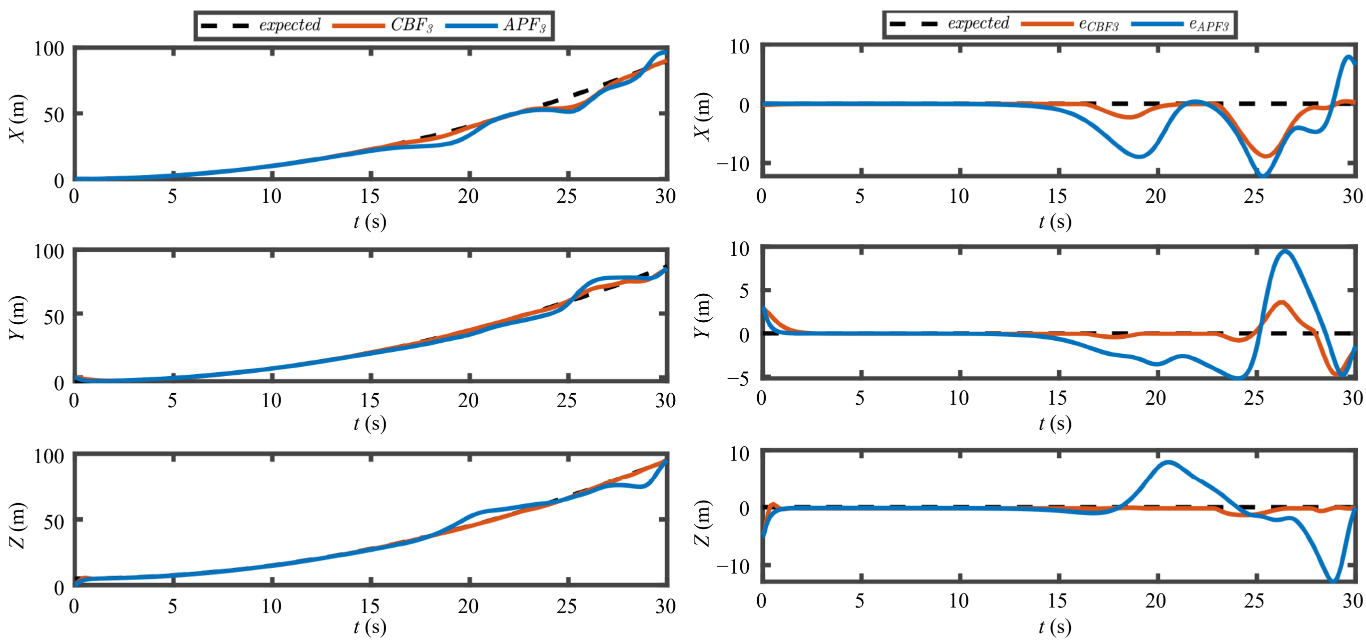

Fig. 8 Comparison tracking results and error for UAV_3 under the CBF and APF.

https://doi.org/10.48130/mav-0026-0014

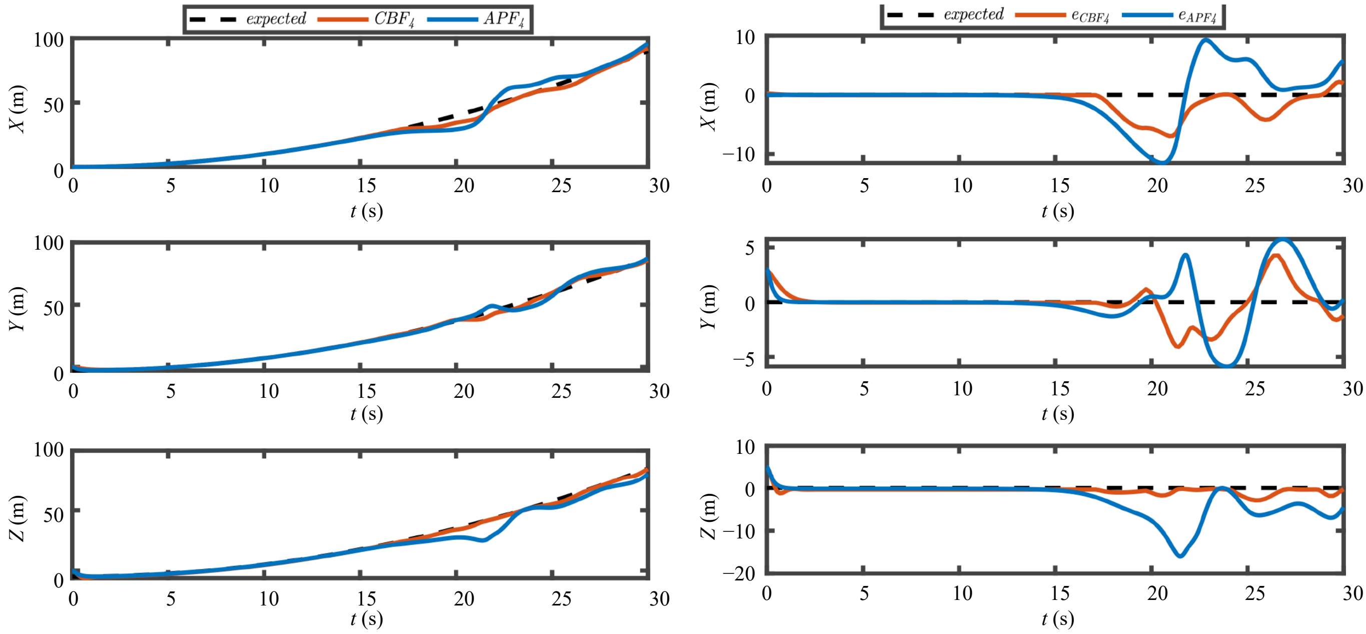

Fig. 9 Comparison tracking results and error for UAV_4 under the CBF and APF.

Table 3. Average MAE of three-axis position.

Method	e_{3x}(m)	e_{3y}(m)	e_{3z}(m)	e_{4x}(m)	e_{4y}(m)	e_{4z}(m)
CBF	1.00	3.19	4.71	3.07	4.40	5.74
APF	4.15	6.23	8.41	2.74	3.73	11.92

Table 4. Average RMSE of three-axis position.

Method	e_{3x}(m)	e_{3y}(m)	e_{3z}(m)	e_{4x}(m)	e_{4y}(m)	e_{4z}(m)
CBF	1.40	3.19	4.71	3.89	4.67	5.76
APF	5.29	6.27	8.89	7.69	4.54	12.81

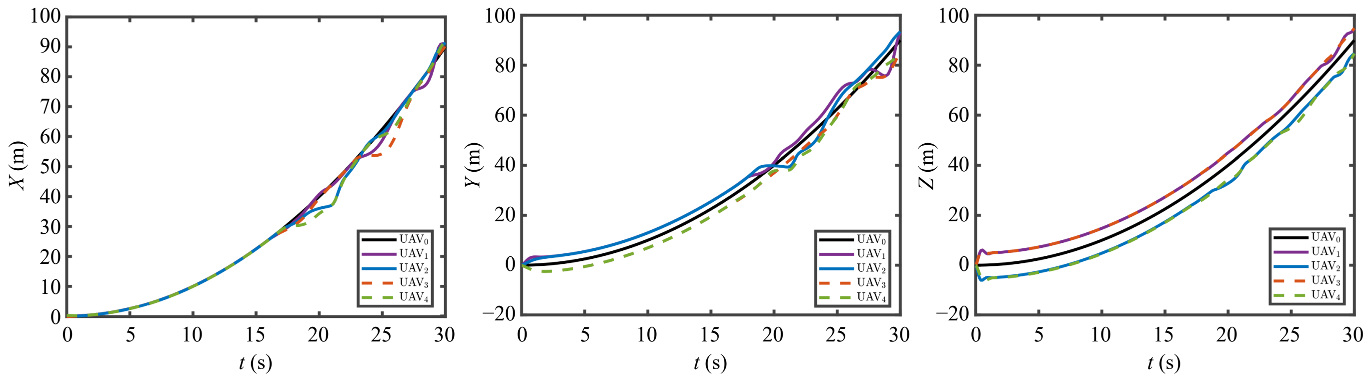

Fig. 10 Three-axis position tracking of UAV formation.

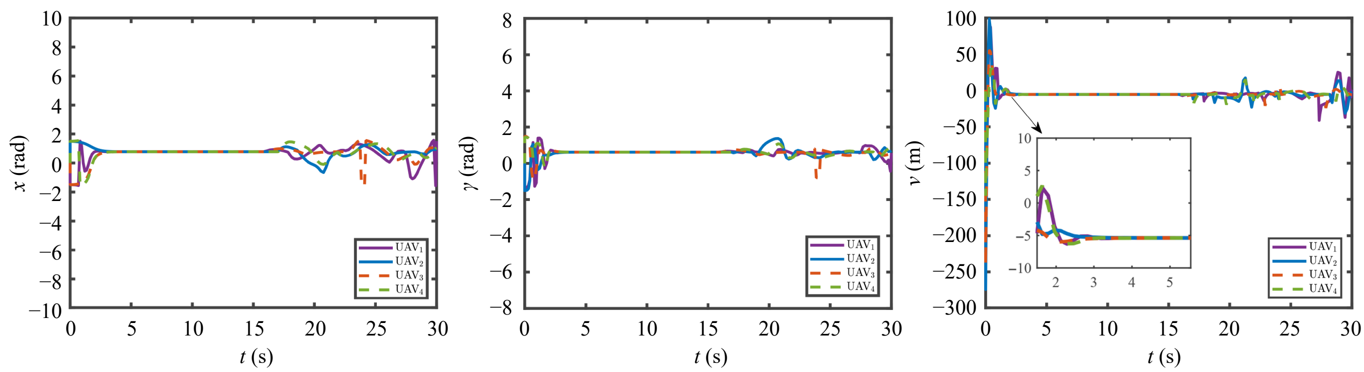

Fig. 11 Flight path angles and speed of the UAV formation.

When encountering obstacles, the UAVs maneuver to avoid them and quickly reconverge to the nominal formation path after passing. Figure 11 provides the time evolution of the flight-path azimuth angle, flight-path angle, and velocity for the four follower UAVs. All followers attain motion synchronization within 5 s. During obstacle avoidance, the states undergo noticeable transients. In particular, the velocity shows a clear deceleration phase when approaching obstacles, followed by a prompt acceleration phase to catch up and restore the commanded formation speed once the obstacles are bypassed.

Conclusions

This work investigates the formation obstacle avoidance issue for MUAVS subject to unknown disturbances. Firstly, the fixed-wing UAV nonlinear dynamic equation is constructed, and the IDO is designed to suppress the adverse impacts of external disturbances on the system. Secondly, a consensus theory-based distributed formation control algorithm is developed to maintain the formation configuration. Meanwhile, to cope with environmental obstacles, a formation collision avoidance strategy is presented by integrating the CBF-QP technique. This strategy allows each UAV to perform timely obstacle avoidance maneuvers and rapidly restore the predefined formation configuration once obstacles are cleared. Finally, Lyapunov stability analysis is conducted to rigorously prove the uniform ultimate boundedness of all closed-loop signals, and numerical simulation results substantiate the superiority of the proposed method. In the future, the issues of real flight experiments, dynamic obstacles, and practical network communication constraints will be further explored in depth.

Author contributions

The authors confirm their contributions to this study as follows: writing – original draft preparation: Wang X, Cao J; writing – review and editing: Yan K; conceptualization: Yan K; resources: Liu D; funding acquisition: Yan K, Liu D; supervision: Sun J. All authors reviewed the results and approved the final version of the manuscript.

Data availability

All data generated or analyzed during this study are included in this published article.

Acknowledgments

This work was supported in part by the National Natural Science Foundation of China under Grant No. 52572455, the Shaanxi Provincial Education Department Service Local Special Plan Project under Grant No. 24JC038, and the 2023 Youth Innovation Team of Shaanxi Universities.

Conflict of interest

The authors declare no conflict of interest.

Dates

Received 20 April 2026; Revised 26 June 2026; Accepted 3 August 2026; Published online 17 September 2026

References

[1] Zhang M, Zhang Y, Mei J. 2025. Integrated guidance law for target tracking and obstacle avoidance in fixed-wing UAVs based on composite system theory. *IEEE Transactions on Vehicular Technology* 74(10):15095−15108

[2] Zhang L, He X, Yu J, Sun S, Yang H. 2025. A distributed time-varying neurodynamic algorithm for multi-UAV collaborative target tracking problem in maritime search and rescue. *ISA Transactions* 167:268−280

[3] Li C, Li G, Song Y, He Q, Tian Z, et al. 2024. Fast forest fire detection and segmentation application for UAV-assisted mobile edge computing system. *IEEE Internet of Things Journal* 11(16):26690−26699

[4] Jia J, Chen X, Wang W, Wu K, Xie M. 2023. Distributed observer-based finite-time control of moving target tracking for UAV formation. *ISA Transactions* 140:1−17

[5] Xia K, Li X, Li K, Zou Y, Zuo Z. 2025. Cooperative tracking of quadrotor UAVs using parallel optimal learning control. *IEEE Transactions on Automation Science and Engineering* 22:3308−3319

[6] Guo J, Liu Z, Song Y, Yang C, Liang C. 2023. Research on multi-UAV formation and semi-physical simulation with virtual structure. *IEEE Access* 11:126027−126039

[7] Yildiz B, Aslan MF, Durdu A, Kayabasi A. 2024. Consensus-based virtual leader tracking swarm algorithm with GDRRT*-PSO for path-planning of multiple-UAVs. *Swarm and Evolutionary Computation* 88:101612

[8] Peng Q, Wu H, Li N, Wang F. 2024. A dynamic task allocation method for unmanned aerial vehicle swarm based on wolf pack labor division model. *IEEE Transactions on Emerging Topics in Computational Intelligence* 8(6):4075−4089

[9] Duan H, Xin L, Shi Y. 2021. Homing pigeon-inspired autonomous navigation system for unmanned aerial vehicles. *IEEE Transactions on Aerospace and Electronic Systems* 57(4):2218−2224

[10] Shi L, Shao J, Cao M, Xia H. 2018. Asynchronous group consensus for discrete-time heterogeneous multi-agent systems under dynamically changing interaction topologies. *Information Sciences* 463:282−293

[11] Wu Y, Gou J, Hu X, Huang Y. 2020. A new consensus theory-based method for formation control and obstacle avoidance of UAVs. *Aerospace Science and Technology* 107:106332

[12] Zhen Z, Tao G, Xu Y, Song G. 2019. Multivariable adaptive control based consensus flight control system for UAVs formation. *Aerospace Science and Technology* 93:105336

[13] Dong X, Hua Y, Zhou Y, Ren Z, Zhong Y. 2019. Theory and experiment on formation-containment control of multiple multirotor unmanned aerial vehicle systems. *IEEE Transactions on Automation Science and Engineering* 16(1):229−240

[14] Huang T, Fan K, Sun W. 2024. Density gradient-RRT: an improved rapidly exploring random tree algorithm for UAV path planning. *Expert Systems with Applications* 252:124121

[15] Erkol O. 2018. Attitude controller optimization of four-rotor unmanned air vehicle. *International Journal of Micro Air Vehicles* 10(1):42−49

[16] Huang S, Zhang H, Huang Z. 2024. E^2CoPre: energy efficient and cooperative collision avoidance for UAV swarms with trajectory prediction. *IEEE Transactions on Intelligent Transportation Systems* 25(7):6951−6963

[17] Wan Y, Zhong Y, Ma A, Zhang L. 2023. An accurate UAV 3D path planning method for disaster emergency response based on an improved multiobjective swarm intelligence algorithm. *IEEE Transactions on Cybernetics* 53(4):2658−2671

[18] Zheng J, Liu K. 2025. 3D UAV trajectory planning with obstacle avoidance for UAV-enabled time-constrained data collection systems. *IEEE Transactions on Vehicular Technology* 74(1):1460−1474

[19] Wang Q, Liu C, Meng Y, Ren X, Wang X. 2024. Reinforcement learning-based moving-target enclosing control for an unmanned surface vehicle in multi-obstacle environments. *Ocean Engineering* 304:117920

[20] Yin M, Li F, Zhao Y, Huang T, Gui W, et al. 2025. Safe cooperative pursuit for multi-UAV systems based on control barrier functions and neurodynamic optimization. *IEEE Transactions on Industrial Informatics* 21(12):9585−9595

[21] Peng C, Liu X, Ma J. 2023. Design of safe optimal guidance with obstacle avoidance using control barrier function-based actor-critic reinforcement learning. *IEEE Transactions on Systems, Man, and Cybernetics: Systems* 53(11):6861−6873

https://doi.org/10.48130/mav-0026-0014

[22] Ko D, Chung W. 2025. A backup control barrier function approach for safety-critical control of mechanical systems under multiple constraints. *IEEE/ASME Transactions on Mechatronics* 30(6):4460−4471
[23] Ma Z, You J, Zhang Y, Cheng Y, Shao J. 2025. Reinforcement learning-based dynamic coverage control of multi-rotor UAVs with safety priority. *IEEE Transactions on Automation Science and Engineering* 22:17474−17485
[24] Jang I, Kim H. 2024. Safe control for navigation in cluttered space using multiple lyapunov-based control barrier functions. *IEEE Robotics and Automation Letters* 9(3):2056−2063
[25] Hung H, Hsu H, Cheng T. 2022. Image-based multi-UAV tracking system in a cluttered environment. *IEEE Transactions on Control of Network Systems* 9(4):1863−1874
[26] Yan S, Shi L, Zhang H, Yao S, Zhou Y. 2023. Safety-critical model-free adaptive iterative learning control for multi-agent consensus using control barrier functions. *IEEE Transactions on Circuits and Systems II: Express Briefs* 71(1):221−225
[27] Ding L, Li Y. 2020. Optimal attitude tracking control for an unmanned aerial quadrotor under lumped disturbances. *International Journal of Micro Air Vehicles* 12:1756829320923563
[28] Huang D, Huang T, Qin N, Li Y, Yang Y. 2022. Finite-time control for a UAV system based on finite-time disturbance observer. *Aerospace Science and Technology* 129:107825
[29] Yong K, Chen M, Wu Q. 2020. Anti-disturbance control for nonlinear systems based on interval observer. *IEEE Transactions on Industrial Electronics* 67(2):1261−1269
[30] Luo M, Su H, Zheng W. 2025. Interval observer-based coordination control for discrete-time multi-agent systems. *IEEE Transactions on Systems, Man, and Cybernetics: Systems* 55(6):4102−4114
[31] Wang X, Su H, Jiang G. 2021. Interval observer-based robust coordination control of multi-agent systems over directed networks. *IEEE Transactions on Circuits and Systems I: Regular Papers* 68(12):5145−5155
[32] Ma L, Zhu F, Zhang J, Zhao X. 2023. Leader-follower asymptotic consensus control of multiagent systems: An observer-based disturbance reconstruction approach. *IEEE Transactions on Cybernetics* 53(2):1311−1323
[33] Zhu X, Li Y, Yin G, Patton RJ. 2024. Interval observer-based fault detection and isolation for quadrotor UAV with cable-suspended load. *IEEE Transactions on Systems, Man, and Cybernetics: Systems* 54(10):5876−5888
[34] Yong K, Chen M, Shi Y, Wu Q. 2022. Flexible performance-based control for nonlinear systems under strong external disturbances. *IEEE Transactions on Cybernetics* 54(2):762−775
[35] Li B, Zhang J, Dai L, Teo KL, Wang S. 2021. A hybrid offline optimization method for reconfiguration of multi-UAV formations. *IEEE Transactions on Aerospace and Electronic Systems* 57(1):506−520
[36] Yan K, Zhang J, Ren H. 2024. Interval observer-based robust trajectory tracking control for quadrotor unmanned aerial vehicle. *International Journal of Control, Automation and Systems* 22(1):288−300
[37] Raissi T, Efimov D, Zolghadri A. 2012. Interval state estimation for a class of nonlinear systems. *IEEE Transactions on Automatic Control* 57(1):260−265
[38] Guo H, Chen M, Shi S, Han Z, Lungu M. 2025. Distributed coordinated control for QUAVs with switching formation strategy. *IEEE Transactions on Intelligent Vehicles* 10(6):3841−3851